Materials and Design 92 (2016) 760–766

Contents lists available at ScienceDirect

Materials and Design

journal homepage: www.elsevier.com/locate/matdes

Effective diffusion coefficient for Cu in steel joined by transient liquid phase bonding

Nicolas Di Luozzo [a,*], Michel Boudard [b], Marcelo Fontana [a], Bibiana Arcondo [a]

[a] Laboratorio de Sólidos Amorfos, INTECIN, Facultad de Ingeniería (UBA-CONICET), Paseo Colón 850, C1063ACV Buenos Aires, Argentina
[b] Laboratoire des Matériaux et du Génie Physique (CNRS UMR 5628), Grenoble Institute of Technology, MINATEC, Grenoble Cedex 1, France

ARTICLE INFO

Article history:
Received 14 August 2015
Received in revised form 15 December 2015
Accepted 17 December 2015
Available online 19 December 2015

Keywords:
Steel
Transient liquid phase bonding
Isothermal solidification
Finite-element simulation
Diffusion kinetic regime

ABSTRACT

Seamless carbon steel tubes were joined by the transient liquid phase (TLP) bonding process using Cu foils as interlayers. Bonding was performed at 1300 °C for 7 min with an applied uniaxial pressure of 5 MPa. The completion of isothermal solidification was not systematically achieved along the joint, leading to the presence of athermally solidified liquid (ASL). Consequently, the ability to predict the time to complete isothermal solidification — and therefore its kinetics — is of great interest. For this purpose, a one-dimensional model using the finite element method was employed to simulate the TLP bonding. In particular, regions where the completion of the process was not achieved provided a source for the effective diffusion coefficient (D_{ef}) for the bonding process. By knowing D_{ef}, different cases were considered within the proposed model, from the remaining time to complete the bonding process for an observed ASL, to the maximum liquid gap that can be isothermally solidified for a selected holding time. The validity of the utilization of D_{ef} was confirmed by analysing the diffusion kinetic regime of Cu in steel.

1. Introduction

Transient liquid phase (TLP) bonding [1] is a joining technique developed as an alternative upon arc welding and brazing (existing bonding methods) and that it improves upon brazing and diffusion bonding, in particular. It involves three main steps, namely, the liquefaction of the interlayer and base metal dissolution, liquid phase isothermal solidification and solute homogenization. This technique has been applied to a wide range of base metals [2–10]: superalloys, steels, aluminium alloys, titanium alloys, pure metals, and between dissimilar metals.

Shimizu et al. [11] first reported several ranges of parameters (roughness of joined surfaces, process temperature (hereafter T_P), holding time at T_P (hereafter t_H), applied pressure, etc.) for TLP bonding of hot-rolled carbon seamless steel tubes with amorphous Ni-based foils as interlayers, for which successful mechanical properties were achieved.

The use of commercially pure Cu foils as interlayers has the advantage of a great range of available shapes and thicknesses, making this option very suitable for industrial application. They were first used by Tuah-Poku et al. [12] for bonding pure Ag rods. In commercial-grade base metals, Assadi et al. [13] first reported their use for aluminium alloy pieces, and Padron et al. [14] for duplex stainless steel blanks.

TLP bonding of hot-rolled carbon seamless steel tubes with Cu interlayers were carried out by Di Luozzo et al. [15]. Tensile tests show that the joined tubes failed away from the joint, attaining almost the ultimate tensile strength of the base metal with a minimal t_H — 7 min. Despite these encouraging results, it appears that the isothermal solidification stage was not systematically completed along the joint, as evidenced by the presence of athermally solidified liquid (ASL). Since the presence of this phase can be detrimental in bending properties and impact strength of the joint, the ability to predict the remaining holding time to complete the TLP bonding through numerical modelling is of great interest.

To gain knowledge of solidification kinetics during TLP bonding, the process was modelled and solved both analytically [12] and numerically [16] considering a one-dimensional (1-D) problem in which local equilibrium at the solid/liquid interface was assumed. Particularly, the finite element method (FEM) proved to be very useful to numerically model moving interfaces [17].

In order to calculate the time to complete the TLP bonding for hot-rolled carbon seamless steel tubes with Cu interlayers, this process is modelled and numerically solved by FEM in the present paper. Particularly, from chemical composition measurements in regions where the completion of the process was not achieved, we are able to obtain the effective diffusion coefficient D_{ef} for the bonding process. The validity of the model assumptions is discussed and the concluding remarks are presented.

2. Experimental

The materials used were hot-rolled carbon seamless steel tubes EN 10297-1 Grade E235, as base metal, and commercially pure Alfa

* Corresponding author.
E-mail address: ndiluozzo@fi.uba.ar (N. Di Luozzo).

http://dx.doi.org/10.1016/j.matdes.2015.12.101
0264-1275/

Table 1
Chemical composition (in wt.%) of the base metal and the interlayer.

	C	Mn	Si	S	P	Cu	Fe
E235 steel	0.12	1.09	0.24	0.0012	0.015	0.049	Bal.
Cu foil[1]						99.973	

[1] O: 0.011 wt.%. The missing balance — 0.016 wt.% — corresponds to impurities not informed in the Certificate of Analysis.

Aesar® Cu foil as interlayer (Table 1). The steel tubes have an outside diameter of 73 mm and a wall thickness of 9.5 mm, while the interlayer has a thickness of 25 μm.

The butted surfaces of the tubes — in the as-machined condition, with a roughness average (R_a) of 10.8 μm — were aligned in contact with the interlayer and placed into the coil of an induction furnace under a controlled reducing atmosphere (10% H_2 + 90% Ar), while a uniaxial pressure of 5 MPa was applied (Fig. 1). The temperature at the joint was raised to $T_P = 1300$ °C, held constant for $t_H = 7$ min, and then was cooled in still air to room temperature. For further details see Di Luozzo et al. [15,17].

Microstructure characterization was carried out with Philips XL30 scanning electron microscope (SEM), and FEI Quanta 250 field-emission gun SEM (FEG-SEM) equipped with a Bruker AXS energy dispersive spectrometer (EDS) — 30 mm^2 active area silicon drift detector — for qualitative chemical composition analysis, using an acceleration voltage of 15 kV.

Quantitative chemical composition analysis was performed with a JEOL JXA 8230 electron probe microanalyzer (EPMA) [18,19], with an operating voltage of 20 kV. The uncertainties in the measurements were computed according to the statistical errors in each point analysis, and they were automatically assessed by the acquisition software (JEOL PC-EPMA 1.9.0.3). Similarly, for a set of point analysis at places where we expected to have similar concentrations, the standard error of the mean was calculated.

Regarding the specimen preparation for both microstructural and chemical characterization, sections perpendicular to CD were analysed.

3. Numerical model

The numerical model for TLP bonding simulations used in this work is described as follows. The model's main assumptions are [12,16,17]:

1. The interface remains planar throughout the process and the initial width of the liquid gap is selected to take into account the variations of its width along the joint. Therefore, the position of the interface can be determined with a unique spatial coordinate and the process can be treated like a one-dimensional (1-D) problem. This assumption is suitable when the base metal is a single crystal [20], or polycrystalline in which an average diffusing atom visits many grains and grain boundaries (GBs) during the annealing time [21]. In the latter case, an effective diffusion coefficient D_{ef} can take into account both volume (in the grain) and GB diffusion.
2. Local equilibrium exists at the solid–liquid interface. Therefore, the concentration of each phase is dictated by a phase diagram — in this particular case, a binary phase diagram. Consequently, the concentration of the solid and the liquid at the interface are the solidus (C_{XS}) and liquidus (C_{XL}) at T_P, respectively.
3. The diffusion coefficients and the molar volume, in the liquid and in the solid, do not depend on solute concentration. Also, the molar volume of each phase does not change during the process.
4. The interface movement is only due to solute diffusion.

For a given time t, the solute concentration $c(x,t)$ and the solid–liquid interface position $X(t)$ are shown in Fig. 2, where x is the distance from the mid-thickness of the liquid gap. The transient liquid phase is limited to $0 \le x < X(t)$, and its total width is $a(t) = 2\,X(t)$. The equations which describe solute diffusion during the TLP boding are [16]:

$$\frac{\partial c_L(x,t)}{\partial t} = D_L \frac{\partial^2 c_L(x,t)}{\partial x^2} \quad 0 < x < X(t) \tag{1}$$

$$\frac{\partial c_S(x,t)}{\partial t} = D_{ef} \frac{\partial^2 c_S(x,t)}{\partial x^2} \quad l > x > X(t) \tag{2}$$

where subscripts L and S indicate the solid and liquid phase, respectively, and l the length of the pieces to be bonded, with $l \gg a(0)$, where $a(0)$ is the initial width of the liquid gap.

The boundary conditions are:

$$\left.\frac{\partial c_L(x,t)}{\partial t}\right|_{x=0} = 0$$

$$\left.\frac{\partial c_S(x,t)}{\partial t}\right|_{x=l} = 0$$

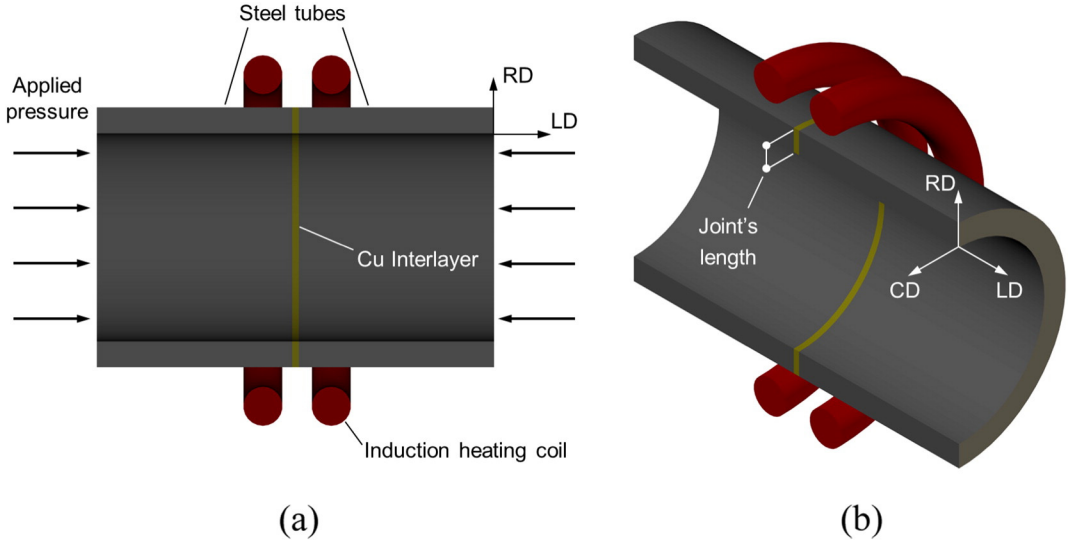

Fig. 1. Schematic illustration of the TLP bonding process: (a) side and (b) perspective section views. The butted surfaces of the tubes to be joined are in contact with the Cu interlayer. The longitudinal direction (LD), radial direction (RD) and circumferential direction (CD) are indicated as well as the joint's length.

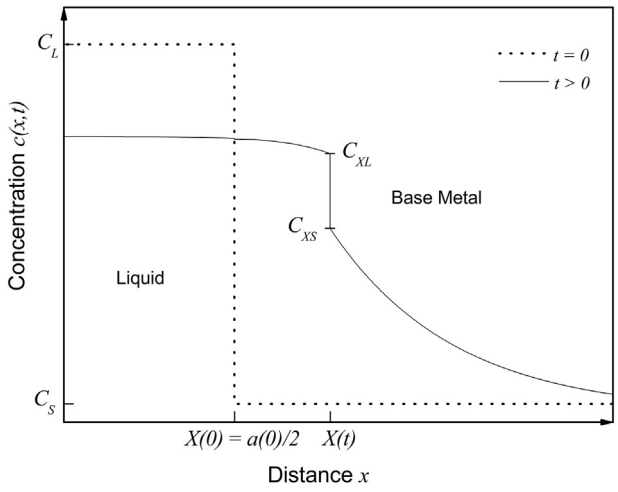

Fig. 2. Solute concentration $c(x,t)$ for $t = 0$ (dotted line) and $t > 0$ (solid line) as a function of the distance from the liquid phase mid-thickness x. The evolution of the solid–liquid interface position with time are indicated by $X(0)$ and $X(t)$.

The initial conditions are:

$$c_L(x,0)=C_L \quad 0 < x < \frac{a(0)}{2}$$

$$c_S(x,0)=C_S \quad l > x > \frac{a(0)}{2}$$

And at the solid–liquid interface:

$$\begin{aligned} c_L(X(t),t)&=C_{XL} \\ c_S(X(t),t)&=C_{XS} \end{aligned} \tag{3}$$

Finally, from mass conservation at the solid–liquid interface, its velocity can be determined:

$$(C_{XL}-C_{XS})\frac{\partial X(t)}{\partial t} = -D_L \frac{\partial c_L(x,t)}{\partial t}\bigg|_{x=X(t)} + D_{ef} \frac{\partial c_S(x,t)}{\partial t}\bigg|_{x=X(t)} \tag{4}$$

This set of equations is solved using FEM in combination with a Crank–Nicholson scheme, in the framework of an iterative process as described in [17].

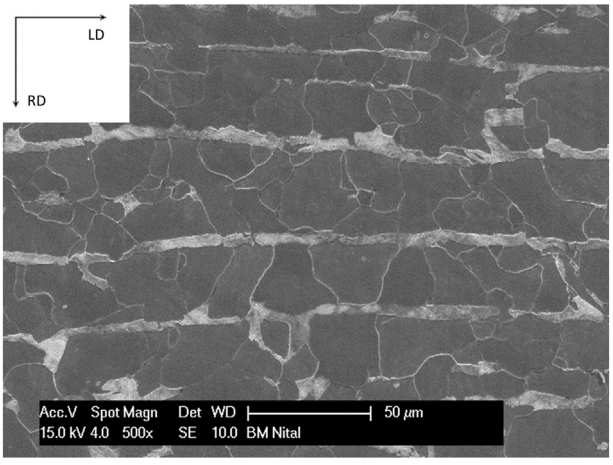

Fig. 3. Microstructure of the base metal. SEM micrograph showing ferrite (dark constituents)/pearlite (bright constituents) bands — secondary electrons, nital etched.

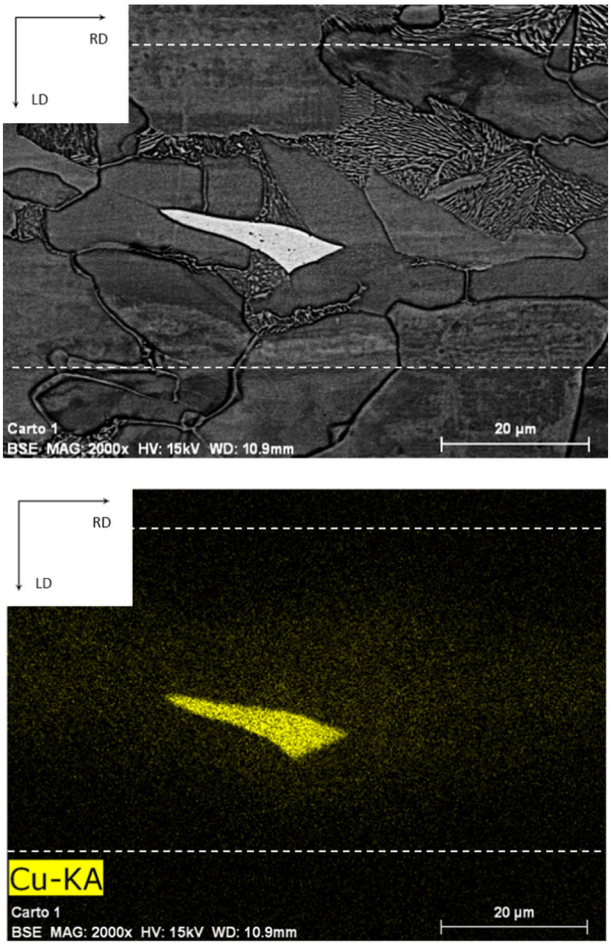

Fig. 4. Top panel: FEG-SEM micrograph at the joint — back scattered electrons, nital etched. Phase with white contrast corresponds to ASL, which is a representative sample of ASL regions. Bottom panel: corresponding Cu mapping (EDS) showing a Cu enriched ferrite adjacent to ASL. The white dotted lines are a guide to the eye of the extension of the joint.

4. Results

4.1. Microstructural characterization

Regarding the base metal, a banded microstructure is observed, containing ferrite and pearlite (Fig. 3). This is intrinsic to the hot-rolling process applied to the seamless steel tubes.

The TLP bonding process was not completely achieved on the whole length of the joint and correspondingly two different microstructures can be observed, as seen in Fig. 4 (Top panel):

- Dark microconstituents correspond to a fully completed process (50–60% of the joint's length[1]). The microstructure presents ferrite and pearlite.
- Light microconstituents are due to an uncompleted process. The microstructure presents a Cu-rich phase, as it was determined from EDS chemical composition mapping of Cu (Fig. 4 (Bottom panel)). This phase — which is randomly scattered throughout the joint — indicates the presence of athermally solidified liquid (ASL), that is, the liquid phase which was unable to solidify isothermally. Regarding their shape, ASLs are strongly stretched in the joint direction, showing maximum widths in the range of 3–5 μm.

[1] The amount of the joint that was completely solidified along the joint's length — the wall thickness of the tube along RD (see Fig. 1) — was chosen to measure the completion of the TLP bonding process.

4.2. Determination of the effective diffusion coefficient D_{ef}

The roughness of the butted surfaces to be joined and the preferential dissolution at GBs of the base metal results in the variation in the width of the TLP along the joint. Consequently, unless the selected t_H is long enough, only some regions can be expected to complete the isothermal solidification stage, while the rest of the joint will have ASL present. Therefore, numerical modelling is one of the most useful tools when estimating isothermal solidification completion time.

For this purpose, chemical composition profiles of solute across the joint of bonded samples can give us valuable information for the TLP bonding process modelling. The region where these solute profiles are carried out is directly related to the information that we can obtain from the model.

In solute profiles obtained from areas where isothermal solidification has finished, the homogenization stage has already begun. Usually, sets of (D_{ef}, $a(0)$) are selected and the extent of the solute homogenization is analysed [14].

Elsewhere, in solute profiles obtained from regions where the isothermal solidification is not completed, we can measure $a(t_H)$ of the ASL from metallographic inspection and the solute profile $c(x,t_H)$ from chemical composition analysis. Therefore, the combination of (D_{ef}, $a(0)$) for which the numerically calculated $a(t_H)$ and $c(x,t_H)$ match with those experimentally measured can be searched.

4.2.1. Chemical composition measurements

The chemical composition was measured by EPMA throughout the ASL and the adjacent base metal. The ASL show an even chemical composition, with a mean value of $Cu_{91.6}Fe_{7.4}Mn_{1.1}$ (in wt.%). The mean chemical composition at 1 μm from the interface in the base metal side was $Fe_{88.8}$ $Cu_{10.6}Mn_{0.4}$ $Si_{0.2}$ (in wt.%).[2,3] The Cu profile adjacent to the ASL, apart from the interface in the base metal — see solid line in Fig. 5 (top panel) — is represented in Fig. 5 (bottom panel).

4.2.2. Numerical simulation

The assigned values for the parameters involved in the numerical simulation are the following:

1. $T_P = 1300$ °C
2. $t_H = 7$ min
3. We assume that the effect of alloying elements in steel — in our case C, Mn and Si — are negligible. Thus, initially, the base metal is composed only of pure Fe — $C_S = 0$ wt.%, and the required equilibrium concentration are obtained from the Cu–Fe phase diagram: the solidus and liquidus composition at T_P are $C_{XL} = 91.0$ wt.% and $C_{XS} = 12.4$ wt.% of Cu, respectively [23].
4. Despite the Cu foil has a width of 25 μm, the applied pressure — of 5 MPa — squeezes out liquid from the joint, including liquid formed during the dissolution stage. Since the dissolution stage is achieved almost instantaneously compared with the isothermal solidification stage [12,24], we assumed that the bonding process starts at the isothermal solidification stage, and that the remaining liquid has already attained the *liquidus* concentration — $C_L = 91$ wt.%.
5. The diffusion coefficient of Fe in liquid Cu is not available. However, self-diffusion coefficients in face-centred cubic metals in the liquid are about 1×10^{-9} to 3×10^{-9} m^2/s at the melting point [21]. Consequently, we assumed an average value of $D_L = 1.5 \times 10^{-9}$ m^2/s.
6. The thickness of the liquid gap at the end of the process is $a(t_H) = 2.54$ μm — the same width measured at the ASL in Fig. 5 (Top panel).

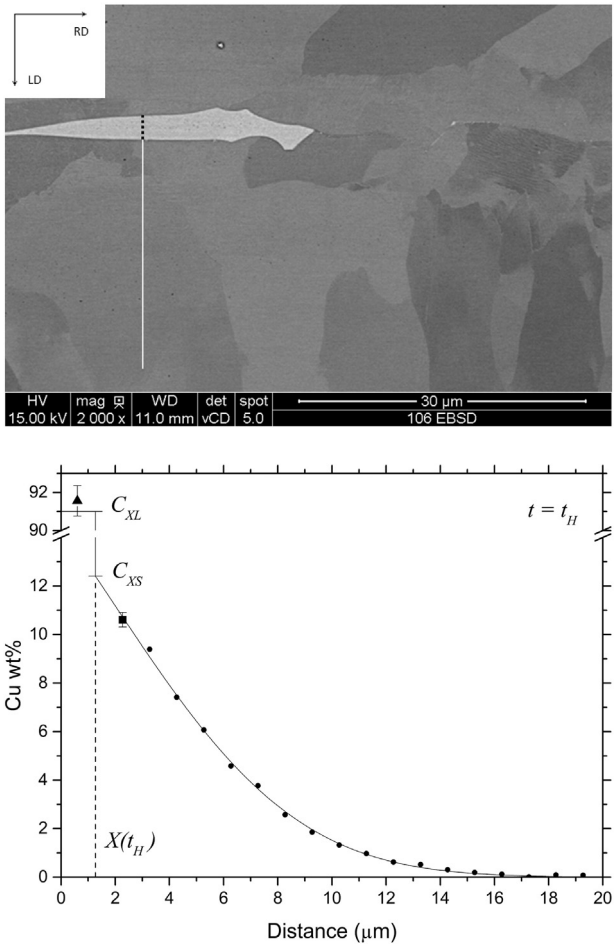

Fig. 5. Top panel: FEG-SEM micrograph at the joint — back scattered electrons, colloidal silica. Light phase corresponds to ASL. The solid line indicates the position of the EPMA profile, and the dotted line indicates the width of the ASL at this position — $a(t_H) = 2.54$ μm; bottom panel: Cu concentration profile as a function of the distance from ASL mid-thickness. Solid line: numerical results for $D_{ef} = 3.48 \times 10^{-14}$ m^2/s, circles: EPMA profile (Error bars are not shown since they are smaller than the data markers), Square: mean EPMA composition at 1 μm from the ASL/base metal interface in the base metal side, Triangle: mean EPMA concentration at ASL. The dashed line indicates the position of the ASL/base metal interface — $X(t_H) = a(t_H)/2 = 1.27$ μm.

The variables to be determined are D_{ef} and $a(0)$, so that the obtained $a(t_H)$ and $c(x, t_H)$ match the measured Cu profile. But each variable can be obtained separately.

Since $D_L \gg D_{ef}$ [21], the liquid phase attains the liquidus concentration almost instantaneously, compared to the kinetics of solid-state diffusion in the base metal. From Eqs. (1) and (4) we have:

$$\frac{\partial c_L(x,t)}{\partial x} \approx 0 \quad 0 < x < X(t)$$

$$\left.\frac{\partial c_S(x,t)}{\partial x}\right|_{x=X(t)} \approx \frac{C_{XL} - C_{XS}}{D_{ef}} \frac{\partial X(t)}{\partial t}$$

Thus, for a given t, the solute concentration gradient at the interface — $\partial c_S(X(t),t)/\partial t$ — depends on its velocity, but not on its position. Furthermore, for a proposed D_{ef} and in combination with Eqs. (2) and (3), we can determine c_S as a function of the distance from the interface, unaffected by the selected $a(0)$. In Fig. 6 we compared Cu concentration profiles in the base metal, measured by EPMA and numerically

[2] This closest distance to the ASL corresponds to the interaction size R of the beam with matter — for pure Fe and an accelerating voltage of 20 kV, $R \approx 1$ μm [22] — and guarantees no contribution from ASL.

[3] Reproducibility of the composition measurement was checked by measuring C_{XL} at different Cu inclusions from 2 different samples (total measurements: 6). The standard error (SE) of the mean of C_{XL} was SE = 0.6 wt.%. Reproducibility was additionally checked by measuring at 1 μm from the interface in the base metal side next to different ASLs from 2 different samples (total measurements: 4). The SE of the mean value was 0.3 wt.%. These values are reported as error bars in Fig. 5. It should be noted that the uncertainties of each measurement of the profile (SE was bounded at 0.1 wt.%) are comparable with those of C_{XL} and at 1 μm from the interface. Therefore, only one EPMA concentration profile was performed.

calculated — assuming $a(0) = 8$ μm and selecting D_{ef} values as multiples of the volume diffusion coefficient of Cu in Fe $D = 2.45 \times 10^{-14}$ m^2/s [25] ($D_{ef} = D, 2D, 4D$ and $10D$). The best D_{ef} value fitting the experimental data appears to be in between D and $2D$ (Fig. 6), and was optimized to $1.42\ D = 3.48 \times 10^{-14}$ m^2/s.

With this selected value of D_{ef}, we searched for a value of $a(0)$ so that $a(t_H) = 2.54$ μm, (see details of the procedure in [16,17]). The obtained value was $a(0) = 3.8$ μm, and the simulated Cu concentration profile is shown in Fig. 5 (Bottom panel), leading to a very good agreement with the experimental measurements.

Furthermore, by knowing D_{ef} we were able to calculate one of the main features of the bonding process: the maximum liquid width that can be isothermally solidified was $a_{max} = 1.25$ μm, for the prescribed $t_H = 7$ min. In other words, due to the irregularities of the solid/liquid interface, wherever the liquid gap was greater than a_{max} led to the presence of ASL at the joint.

Additionally, the time to complete the isothermal solidification process t_{Iso} was calculated. For the assumed $a(t_H) = 2.54$ μm, we obtained $t_{Iso} = 58$ min $\approx 8\ t_H$.

5. Discussion

We discuss hereafter the important hypothesis used in the model.

5.1. Local equilibrium at the solid–liquid interface and the transient liquid phase composition

The ASL is a Cu-rich phase (Fig. 4 (bottom panel)), whose even concentration is almost coincident with C_{XL} at T_P (Fig. 5 (bottom panel)). Furthermore, the chemical composition of the ASL/base metal interface — in the base metal side — converges to C_{XS}. These results show the suitability of the assumptions made in the TLP bonding process modelling for our particular case, regarding:

- Local equilibrium at the solid/liquid interface.
- The completion of the dissolution stage is achieved almost instantaneously, and at the end of this stage the transient liquid phase attained an even C_{XL} concentration.

5.2. Suitability of the 1-D problem approximation

With the aim to ensure the validity of D_{ef} calculated in Section 4.2.2, the suitability of the 1-D problem approximation has to first be analysed. For this purpose, the diffusion kinetic regime of the solute in the base metal was studied [21]. It is accomplished by determining a set of variables, which are obtained in three steps:

1. The critical penetration depth at the grain L' and GB L'', which allows us to determine if the polycrystal could be assumed as a fine-grained or coarse-grained polycrystal [26].
2. The adimensional variable β associated with the shape of isoconcentration contours at GBs — the larger the value of β, the more pronounced is the diffusion along GBs [27] — and the characteristic time at the grain t' and GB t'', to be compared with the experimental holding time t_H [28].
3. The characteristic diffusion length at the grain L and GB L_b, which is compared to the average grain size d [26]. In our case, d is estimated to be 25 μm by microstructural analysis.

Beginning with the classification of the base metal by means of d, L' and L''[4]:

$$d \approx 25\ \mu m$$

$$L' = \frac{\delta}{2}\left(\frac{D_b}{D}\right)^{1/2} = 22.2\ nm$$

$$L'' = \frac{\delta}{2}\frac{D_b}{D} = 1.97\ \mu m$$

where D_b is the GB diffusion coefficient estimated in 1.93×10^{-10} m^2/s [29], and $\delta = 0.5$ nm is the thickness of GBs [30]. Since $d \approx L'$ and $d > L''$, we conclude that the base metal can be considered a coarse-grained polycrystal [26].

Mishin et al. [28] proposed a complete classification of diffusion regimes for coarse-grained polycrystals considering the variables β, t' and t''. We can obtain:

$$\beta = \frac{\delta D_b}{2D(Dt_H)^{1/2}} = 0.614$$

$$t' = \frac{\delta^2}{4D} = 2.55\ \mu s$$

$$t'' = \frac{(\delta D_b)^2}{4D^3} = 159\ s$$

We can approximate these results as $\beta \approx 1$, $t_H \gg t'$ and t_H is on the same order of magnitude as t'', that characterize the diffusion kinetic regime as B_3. In this regime, the penetration depth of the solute to the GB and to the volume is comparable.

Furthermore, from the characteristic diffusion lengths L and L_b we obtained:

$$L = (Dt_H)^{1/2} = 3.21\ \mu m$$

$$L_b = \frac{(\delta D_b)^{1/2}}{(4D/t_H)^{1/4}} = 2.51\ \mu m$$

Thus, we obtain the conditions $L \approx L_b$ and $d > L, L_b$. These results and previous works (e.g.: [26]) shows that the B_4 regime — which is characterized by the predominance of volume diffusion — is almost reached.

We can conclude that the diffusion kinetic regime of the base metal was transitioning from B_3 to B_4. Therefore, diffusing atoms were practically not confined to any particular GB. Thus, the 1-D problem approximation is applicable.

It should be kept in mind that at the initial stage of TLP bonding process, a liquid gap extends throughout the joint, whose interfaces can be assumed planar. Therefore, the 1-D problem approximation makes sense — in other words, diffusion takes place perpendicular to

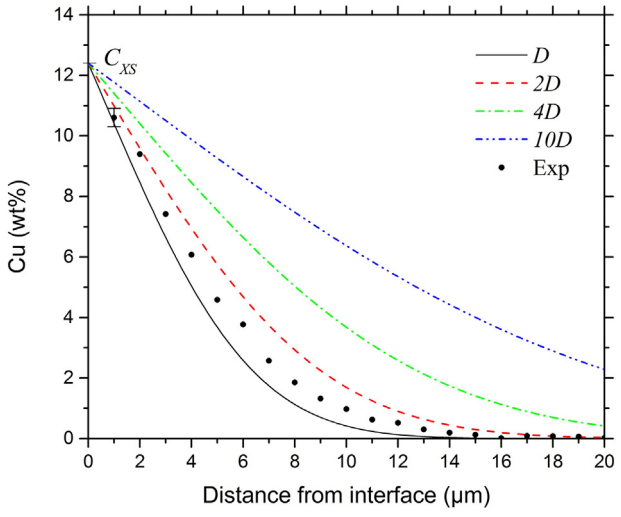

Fig. 6. Cu concentration profiles in the base metal vs. distance from ASL/base metal interface. Lines: numerically calculated (as a function of D_{ef}); circles: experimentally measured (by EPMA — error bars not shown are smaller than the data markers).

[4] For sake of simplicity, segregation effects on GB diffusion were not taken into account [27].

the joint. At a later stage of the process, the remaining liquid gaps at the joint — which resemble the ASLs — are surrounded three-dimensionally by the base metal. In particular, regarding their shape, they are strongly stretched in the joint direction as ASLs, as it is shown in Fig. 4 (top panel) and Fig. 5 (top panel). Again, it is assumed that diffusion takes place mostly perpendicular to the joint, and boundary effects associated with the ends of the liquid gaps are not taken into account.

5.3. Holding time t_H vs. time to complete the isothermal solidification process t_{Iso}

From the analysed results we obtained that, during the TLP bonding, the process could be assumed as a 1-D problem, with a coefficient $D_{ef} = 3.48 \times 10^{-14}$ m^2/s — which is close to D.

This result is in contrast with most of the existing literature. For example, Tuah-Poku et al. [12] determined experimentally the completion of the isothermal solidification stage in ≈200 h in Ag/Cu/Ag joints. However, they predicted $t_{Iso} \approx 1200$ h, ascribing this discrepancy mostly to the curved nature of the interface. MacDonald et al. [24] reported similar differences between the experimentally measured and calculated t_{Iso} in Cu/Ag–28Cu/Cu joints (in wt.%): ≈300 h and 1393 h respectively, which was associated to the formation of regions of enhanced diffusivity along GBs. In TLP bonded duplex stainless steel (DSS) pieces, Padron et al. [14] assumed an unrealistically high $D_{ef} = 1.437 \times 10^{-12}$ m^2/s at 1100 °C for Cu in DSS/Cu/DSS joints to match the calculated and experimentally measured t_{Iso}. It was attributed to enhanced Cu diffusivity in α-Fe in the α-Fe/γ-Fe base metal matrix.

But it was the existence of a variable liquid gap along the joint that became the greatest drawback in calculating the time for completion of the isothermal solidification stage. This was directly connected with the roughness of the butted surfaces to be joined and the preferential dissolution at GBs of the base metal. As a result, a liquid gap with an irregular width took place.

The same difficulties are encountered in our paper. As we can see in Figs. 4 and 5, the isothermal solidification of the liquid gap was achieved in most of the joint. From numerical modelling, we obtained that in this cases the liquid gap was up to 1.25 μm. However, if we want to complete the isothermal solidification for the observed ASL in Fig. 5 (top panel), $t_{Iso} \approx 8\ t_H$.

Regarding the roughness of the butted surfaces, the measured R_a in the as-machined condition is prominent. However, their roughness during TLP bonding decreases significantly. Under the applied pressure at T_P, surface peaks are plastically compressed, reducing its roughness during bonding. Therefore, the solid–liquid interfaces of the liquid gap at the onset of the solidification are largely planar, supporting the 1-D model approximation. Anyway, its influence cannot be directly measured — it can only be qualitatively analysed by metallographic inspection [31].

Concerning the precision of the calculated t_{Iso}, we should bear in mind that it is strongly connected with the fulfilment of the model's assumptions in each of the studied systems. In this work, for example, we assumed that the diffusion coefficient of Cu in Fe is independent of its concentration, and equal to the impurity diffusion of Cu in polycrystalline Fe at T_P [25]. This was only reported when the concentration of Cu is less than 4.5 wt.% in the temperature range of 929–1020 °C [32], and may become, if not fulfilled, a source of error.

Therefore, for a given t_H, we can observe from metallographic inspection if the isothermal solidification stage is complete or not. In the latter case, D_{ef} can be calculated with the procedure presented in this paper, and t_{Iso} can be determined from the measured widths of the observed ASL.

6. Conclusions

Hot-rolled carbon seamless steel tubes were TLP-bonded, with pure Cu foils as interlayer. The obtained joints were both microstructurally and chemically characterized. It was observed that the isothermal solidification stage was not systematically achieved along the joint, which led to the presence of ASL. To analyse the kinetics of the bonding process, the steel/Cu/steel joint was numerically modelled, and the analysis of both numerical results and experimental measurements was carried out, which lead to the following main conclusions:

1. The assumption of local equilibrium at the solid/liquid interface during the TLP bonding process proved to be completely suitable. The liquidus concentration at the process temperature was practically reached at the ASL. On the other hand, the measured chemical composition of the ASL/base metal interface — in the base metal side — converges to the solidus concentration.
2. From the diffusion kinetic analysis of the base metal, we can conclude that the base metal is transitioning from B_3 to B_4 regime. Therefore, volume diffusion dominates diffusion in the base metal. Accordingly, TLP bonding modelling can be assumed as a 1-D problem, and a D_{ef} for the polycrystalline base metal can be calculated.
3. Numerical results matched the experimentally measured Cu concentrations for $D_{ef} = 1.42\ D$. This value, which is close to D, was obtained analysing a region at the joint where the isothermal solidification was not completed.
4. A liquid gap with an irregular width takes place due to surface roughness of the butted surfaces to be joined and liquid penetration at grain boundaries. Where isothermal solidification stage is not completed for the selected t_H, D_{ef} can be determined, making it possible to calculate t_{Iso}.

Acknowledgments

This work was supported by the Universidad de Buenos Aires, Grant No. 20020130100515BA. The authors wish to thank Dr. Gustavo Castellano (FaMAF, UNC — CONICET) for his helpful discussions.

References

[1] D.F. Paulonis, D.S. Duvall, W.A. Owczarski, Inventors; United Aircraft Corp., Assignee, Diffusion bonding utilizing transient liquid phaseUnited States patent US 3678570 July 25 1972.
[2] G.O. Cook, C.D. Sorensen, Overview of transient liquid phase and partial transient liquid phase bonding, J. Mater. Sci. 46 (2011) 5305–5323.
[3] S. Shakerin, H. Omidvar, S.E. Mirsalehi, The effect of substrate's heat treatment on microstructural and mechanical evolution of transient liquid phase bonded IN-738 LC, Mater. Des. (2015)http://dx.doi.org/10.1016/j.matdes.2015.10.003.
[4] J. Cao, Y.F. Wang, X.G. Song, C. Li, J.C. Feng, Effects of post-weld heat treatment on microstructure and mechanical properties of TLP bonded inconel 718 superalloy, Mater. Sci. Eng. A 590 (2014) 1–6.
[5] S. Steuer, R.F. Singer, Suppression of boride formation in transient liquid phase bonding of pairings of parent superalloy materials with different compositions and grain structures and resulting mechanical properties, Metall. Mater. Trans. A 45A (2014) 3545–3553.
[6] V. Jalilvand, H. Omidvar, M.R. Rahimipour, H.R. Shakeri, Influence of bonding variables on transient liquid phase bonding behavior of nickel based superalloy IN-738LC, Mater. Des. 52 (2013) 36–46.
[7] M. Pouranvari, A. Ekrami, A.H. Kokabi, Transient liquid phase bonding of wrought IN718 nickel based superalloy using standard heat treatment cycles: microstructure and mechanical properties, Mater. Des. 50 (2013) 694–701.
[8] X. Zhou, Y. Dong, C. Liu, Y. Liu, L. Yu, J. Chen, H. Li, J. Yang, Transient liquid phase bonding of CLAM/CLAM steels with Ni-based amorphous foil as the interlayer, Mater. Des. 88 (2015) 1321–1325.
[9] J. Ruiz-Vargas, N. Siredey-Schwaller, N. Gey, P. Bocher, A. Hazotte, Microstructure development during isothermal brazing of Ni/BNi-2 couples, J. Mater. Process. Technol. 213 (2013) 20–29.
[10] X. Wang, X. Li, C. Wang, Effect of two-step heating process on joint microstructure and properties during transient liquid phase bonding of dissimilar materials, Mater. Sci. Eng. A 560 (2013) 711–716.
[11] T. Shimizu, H. Horio, K. Kitou, S. Inagaki, R. Yamada, Inventors; Daido Tokushuko Kabushiki Kaisha, Assignee, Method for manufacturing joint of carbon steel pipes suitable for expansion and expanding methodUnited States patent US 6378760 Apr 30 2002.
[12] I. Tuah-Poku, M. Dollar, T. Massalski, A study of the transient liquid phase bonding process applied to a Ag/Cu/Ag sandwich joint, Metall. Trans. A 19A (1988) 675–686.
[13] H. Assadi, A.A. Shirzadi, E.R. Wallach, Transient liquid phase diffusion bonding under a temperature gradient: modelling of the interface morphology, Acta Mater. 49 (2001) 31–39.

[14] T. Padron, T.I. Khan, M.J. Kabir, Modelling the transient liquid phase bonding behaviour of a duplex stainless steel using copper interlayers, Mater. Sci. Eng. A 385 (2004) 220–228.
[15] N. Di Luozzo, M. Boudard, B. Doisneau, M. Fontana, B. Arcondo, Transient liquid phase bonding of carbon steel tubes using a Cu interlayer: characterization and comparison with amorphous Fe–B–Si interlayer bonds, J. Alloys Compd. 615 (2014) S13–S17.
[16] Y. Zhou, T.H. North, Kinetic modelling of diffusion-controlled, two-phase moving interface problems, Model. Simul. Mater. Sci. Eng. 1 (1993) 505–516.
[17] N. Di Luozzo, M. Fontana, B. Arcondo, Transient liquid phase bonding of steel using an Fe–B interlayer, J. Mater. Sci. 42 (2007) 4044–4050.
[18] J. Goldstein, D.E. Newbury, D.C. Joy, C.E. Lyman, P. Echlin, E. Lifshin, et al., Scanning Electron Microscopy and X-ray Microanalysis, third ed. Springer, New York, 2003.
[19] S.J.B. Reed, Electron Microprobe Analysis and Scanning Electron Microscopy in Geology, second ed. Cambridge University Press, Cambridge, 2005.
[20] K. Saida, Y. Zhou, T.H. North, The influence of base metal grain size on isothermal solidification during transient liquid-phase brazing of nickel, J. Mater. Sci. 28 (1993) 6427–6432.
[21] Y. Mishin, C. Herzig, Grain boundary diffusion: recent progress and future research, Mater. Sci. Eng. A 260 (1999) 55–71.
[22] K. Kanaya, S. Okayama, Penetration and energy-loss theory of electrons in solid targets, J. Phys. D Appl. Phys. 5 (1972) 43–58.
[23] H. Baker, ASM Handbook Volume 3 — Alloy Phase Diagrams, 10th ed. ASM International, Materials Park, 1992.
[24] W. MacDonald, T. Eagar, Isothermal solidification kinetics of diffusion brazing, Metall. Mater. Trans. A 29A (1998) 315–325.
[25] S.J. Rothman, The diffusion of copper in iron, J. Appl. Phys. 39 (1968) 5041–5044.
[26] Y. Mishin, C. Herzig, Diffusion in fine-grained materials: theoretical aspects and experimental possibilities, Nanostruct. Mater. 6 (1995) 859–862.
[27] I. Kaur, Y. Mishin, W. Gust, Fundamentals of Grain and Interphase Boundary Diffusion, third ed. Wiley, Chichester, 1995.
[28] Y. Mishin, I.M. Razumovskii, Analysis of an asymmetrical model for boundary diffusion, Acta Metall. Mater. 40 (1992) 597–606.
[29] A.M. Brown, M.F. Ashby, Correlations for diffusion constants, Acta Metall. 28 (1980) 1085–1101.
[30] J. Fisher, Calculation of diffusion penetration curves for surface and grain boundary diffusion, J. Appl. Phys. 22 (1951) 74–77.
[31] N. Di Luozzo, M. Fontana, B. Arcondo, Transient liquid phase bonding of steel using an Fe–B interlayer: microstructural analysis, J. Mater. Sci. 43 (2008) 4938–4944.
[32] Y. Liu, J. Wang, Y. Du, L. Zhang, D. Liang, Mobilities and diffusivities in fcc Fe–X (X = Ag, Au, Cu, Pd and Pt) alloys, Calphad 34 (2010) 253–262.